NATIONAL ADVISORY COMMITTEE FOR AERONAUTICS

TECHNICAL NOTE 3394

LOW-SPEED INVESTIGATION OF THE EFFECTS OF ANGLE OF ATTACK ON THE PRESSURE RECOVERY OF A CIRCULAR NOSE INLET WITH SEVERAL LIP SHAPES

By James R. Blackaby

Ames Aeronautical Laboratory
Moffett Field, Calif.

Washington
May 1955

NATIONAL ADVISORY COMMITTEE FOR AERONAUTICS

TECHNICAL NOTE 3394

LOW-SPEED INVESTIGATION OF THE EFFECTS OF ANGLE OF ATTACK ON THE PRESSURE RECOVERY OF A CIRCULAR NOSE INLET WITH SEVERAL LIP SHAPES

By James R. Blackaby

SUMMARY

Wind-tunnel tests were conducted to ascertain the total-pressure recovery of a circular nose inlet utilizing various shapes of inlet lips. The tests were conducted at a free-stream Mach number of 0.237 with inlet flows ranging from low values to choking and at angles of attack from 0° to 25°.

A sharp inlet lip having a wedge angle of 7-1/2° was tested in addition to two circular-arc profiles and two elliptical profiles formed within the wedge of the sharp lip by cutting back the leading edge various amounts. It was found that for a given amount of cutback, the circumferential variation of total pressure at the measuring station (the simulated entrance to a turbojet-engine compressor) was about the same with either an elliptical- or circular-arc-profile lip; however, the average total-pressure recovery characteristics were better with the elliptical-profile lip.

INTRODUCTION

In reference 1, the results are presented of an investigation of some of the effects of lip shape on the low-speed characteristics of circular nose inlets at an angle of attack of 0°. In practice, the low subsonic speeds and the high mass-flow ratios covered in those tests are associated with the moderate to high angles of attack occurring during landing or take-off. The present report covers an extension of the investigation reported in reference 1 to include the measurement of the effects of angle of attack on the total-pressure recovery at the entrance to the simulated turbojet-engine compressor in the wind-tunnel model.

The body of revolution and five of the inlet-lip profiles of reference 1 were utilized in the present tests. The lip profiles included the sharp lip, two of the lips with circular-arc profiles (providing inlet contraction ratios, that is, the ratio of the area encompassed by the leading edge of the inlet to the minimum inlet area, of 1.16 and 1.33), and the two lips with elliptical profiles (providing contraction ratios of 1.08 and 1.18). The tests were conducted in one of the Ames 7- by 10-foot wind tunnels.

NOTATION

The following symbols and subscripts are used in this report:

A	area, sq ft
H	total pressure, lb/sq ft
M	Mach number
m	mass-flow rate, ρAV, slugs/sec
m_o	reference mass-flow rate, $\rho_o A_1 V_o$, slugs/sec
q	dynamic pressure, lb/sq ft
r	radius, in.
V	air velocity, ft/sec
x	axial distance, in.
y	ordinate, measured normal to body axis, in.
α	angle of attack, deg
ρ	mass density of air, slugs/cu ft

Subscripts

l	local conditions at the face of the total-pressure rake, station 36.25 (fig. 1)
o	conditions in the free stream

1 average conditions at the exit of the constant-area portion of the inlet, station 15.00 (A_1 = 0.0942 sq ft)

3 average conditions at the face of the total-pressure rake, station 36.25 (A_3 = 0.1389 sq ft)

MODEL AND TESTS

The model used in the tests was a streamline body of revolution with internal ducting and provisions for mounting interchangeable inlet portions at the nose (figs. 1, 2, and 3). The body, which had a maximum diameter of 12 inches at station 72.00, was mounted on an 8-inch-diameter vertical strut through which the inlet air flow was exhausted. The total length of the body was 129 inches.

The inlet portions (fig. 2) were machined from aluminum or brass castings, and the lip profiles were formed within the boundaries of a basic sharp-edged inlet. This sharp-edged inlet was formed with a conical outer surface, tangent to the basic forebody at station 14.118, and with a cylindrical inner surface with a radius of 2.078 inches extending from the sharp leading edge, station 9.00, to station 15.00. The angle between the inner and outer surfaces was about 7-1/2°.

In addition to the sharp-edged inlet, two with circular-arc profiles and two with elliptical internal and approximately elliptical external profiles were tested. (The two types of profiles will be referred to as circular type and elliptical type in the rest of the report.) The profiles are identified by numbers and letters as shown in figure 2. The number is approximately equal to the decimal portion of the inlet contraction ratio while the letter R indicates a circular profile and the letter E, an elliptical profile. Thus, lip 16R had a circular profile and the area encompassed by the leading edge was about 16-percent (actually 15.8 percent, as tabulated in fig. 2) greater than the minimum inlet area. The minimum inlet area was equal to 12 percent of the maximum frontal area of the body.

The diffusion ratio of the internal duct (A_3/A_1) was 1.474. The included angle of the unobstructed conical portion of the diffuser - from station 15.00 to station 32.00 - was about 4°.

The air flow through the inlet and subsequent ducting was regulated by an exhaust pump outside the wind-tunnel test chamber. The rate of inlet air flow was measured by a calibrated orifice meter, and the loss of total pressure from the free stream to the simulated turbojet-engine compressor inlet, station 3 (station 36.25, fig. 1), was measured by a rake consisting of 24 total-pressure and 4 static-pressure tubes. The total-pressure loss was measured for mass-flow ratios m_1/m_0 from 0.6 to choking for each lip for angles of attack of 0°, 5°, 10°, 15°, 20°, and 25°. The test Mach

number was 0.237, corresponding to a dynamic pressure of 80 pounds per square foot and a Reynolds number of 136,000 per inch. No tunnel-wall corrections were applied to any of the data.

RESULTS AND DISCUSSION

The variations of average total-pressure ratio H_3/H_0 and mass-flow ratio m_1/m_0 with the Mach number at the simulated compressor entrance M_3 are presented in figures 4(a) through 4(f) for each lip and each test angle of attack. A comparison of the characteristics for the inlet with the various types of lips shows that, in general, for all the lips there was a decrease of total-pressure ratio as either mass-flow ratio or angle of attack was increased (an exception, which will be discussed below, occurred with lip 33R at an angle of attack of 20°). However, the elliptical lips demonstrated an ability to maintain higher total-pressure ratios over a limited range of mass-flow ratios or angles of attack than did corresponding circular lips. ("Corresponding lips" refer to elliptical and circular lips having about the same contraction ratios which were formed by cutting back the basic sharp lip approximately equal amounts.) Thus, the total-pressure ratio measured with lip 8E remained as high as that with lip 33R up to a mass-flow ratio of about 1.6 ($M_3 \approx 0.27$) at $\alpha = 0°$ and up to a mass-flow ratio of about 1.4 ($M_3 \approx 0.23$) at $\alpha = 5°$. Similarly, the total-pressure ratio measured with lip 18E remained about the same as that with lip 33R throughout the range of mass-flow ratios for angles of attack of 0° and 5°, and up to a mass-flow ratio of about 1.6 ($M_3 \approx 0.27$) at $\alpha = 10°$ and 1.4 ($M_3 \approx 0.23$) at $\alpha = 15°$. For both of the elliptical lips, the range of high total-pressure ratios terminated abruptly, probably as a result of an abrupt separation of the inlet flow from the inner surface of the lips.

For lip 33R at an angle of attack of 20°, the internal flow, which is believed to have been separated from the lower portion of the lip at the lowest mass-flow ratios, appears to have reattached above $m_1/m_0 = 1.0$ ($M_3 \approx 0.16$) and high total-pressure ratios were measured until separation again occurred above $m_1/m_0 = 1.9$ ($M_3 \approx 0.31$). The total-pressure ratios for lip 33R at high mass-flow ratios at $\alpha = 20°$, and over the entire mass-flow range at $\alpha = 25°$, were approximately the same as those for lip 18E. (With lip 33R it was possible to attain a total-pressure ratio greater than 0.99 for the intermediate mass-flow ratios - near $m_1/m_0 = 1.6$ - for angles of attack as high as 25°. This was accomplished by setting the mass-flow ratio at an angle of attack below 20°, then increasing α. The flow conditions thus established in the inlet were unstable at 25°, however, and either raising or lowering the mass-flow ratio a small amount induced separation of the inlet flow and the characteristics reverted to those shown in figure 4(b).)

Figure 5, which includes crossplots of the faired curves of figure 4, provides a graphic picture of the increasing superiority of the blunt lips over the sharp lip, and of lips 18E and 33R over lips 16R and 8E, at all angles of attack as the mass-flow ratio was increased to choking values. The total-pressure ratios for high angles of attack and for high mass-flow ratios should be considered as qualitative data only because of the inherent inaccuracy of total-pressure measurements by means of impact tubes in regions of unsteady flow, such as those which exist at high angles of attack due to flow separation from the lips and those which were shown in reference 1 to exist at high mass-flow ratios. The maximum, or choking, mass-flow ratios from the curves of figures 4(a) through 4(f) were utilized in figure 6 to show the small variation of the choking mass-flow ratio with angle of attack for each of the lips.

The effects of increasing the angle of attack on the total-pressure ratio at the simulated turbojet-engine compressor entrance were evidenced, not only by the reduction of the average total-pressure ratios H_3/H_0, but also by an asymmetry of the contours of total-pressure ratio H_1/H_0. This flow asymmetry may have a large effect on the performance of a turbojet engine, and the extent to which the asymmetry is affected by lip profile is illustrated in figures 7 and 8 where faired contours of total-pressure ratio are presented. Examples are included for each of the lips for angles of attack of 0°, 15°, and 25° (0°, 20°, and 25° for lip 33R for $m_1/m_0 \approx 1.6$) for a mass-flow ratio of about 1.6 (fig. 7) and for the critical mass-flow condition (fig. 8).

Inspection of the figures reveals that the maximum circumferential variation of local total-pressure ratio occurred, in most cases, at a radius of about 2 inches (the radius of the center body was 1.261 inches and the radius to the duct wall was 2.822 inches as shown in fig. 1) for the high-angle-of-attack cases presented. In general, the pressure variations measured with lips 16R and 18E were of about equal magnitude for the various conditions presented but were somewhat larger than those with lip 33R. The greatest pressure variations were, of course, measured with lips 8E and 0. It can be seen from figures 7 and 8 that the separation of the internal flow from the lower portion of the lips at angles of attack of 15° and 25° resulted, in general, in a region of low total pressures in the lower portion of the duct and a region of comparatively high pressures in the upper portion. An exception to this general trend occurred in the case of lip 33R at the critical mass-flow ratio (fig. 8(c)); the reasons for this exception are not apparent.

Contour plots are included in figures 9, 10, and 11 to illustrate the flow changes at the simulated engine-compressor entrance for selected conditions for the inlet with three of the lips. The change from a symmetric to an asymmetric flow condition with lip 18E is shown in figure 9 where the contour plots for an angle of attack of 15° and mass-flow ratios of 1.44 and 1.51 are presented. The decrease of the average total-pressure ratio H_3/H_0 accompanying the flow change was noted previously in figure

4(d). Similarly, the flow changes accompanying the total-pressure loss suffered with lip 33R between the mass-flow ratios of 1.87 and 2.08 at an angle of attack of 20° (fig. 4(e)) are illustrated in figure 10.

In figure 11, the flow changes accompanying the choking of the inlet with lip 0 at $\alpha = 0°$ are shown. The three conditions included correspond with high subcritical, critical, and supercritical inlet flow ($M_3 = 0.37$, 0.41, and 0.46, respectively). For the subcritical and supercritical conditions the lowest total pressures were measured at the outer wall of the duct with H_l/H_o increasing steadily across the annular duct to the highest values, which were measured adjacent to the center body. Near the critical inlet-flow conditions, however, losses appear to have occurred in the center of the duct, perhaps as a result of the shock waves in the center of the inlet discussed in reference 1, or as a result of a temporary separation of the flow from the center body. Whatever the cause, the effect was an annular peak in the total-pressure ratio at a radius of about 1.85 inches, with lower pressures at the duct wall and adjacent to the center body.

National Advisory Committee for Aeronautics
Ames Aeronautical Laboratory
Moffett Field, Calif., Mar. 21, 1955

REFERENCE

1. Blackaby, James R., and Watson, Earl C.: An Experimental Investigation at Low Speeds of the Effects of Lip Shape on the Drag and Pressure Recovery of a Nose Inlet in a Body of Revolution. NACA TN 3170, 1954.

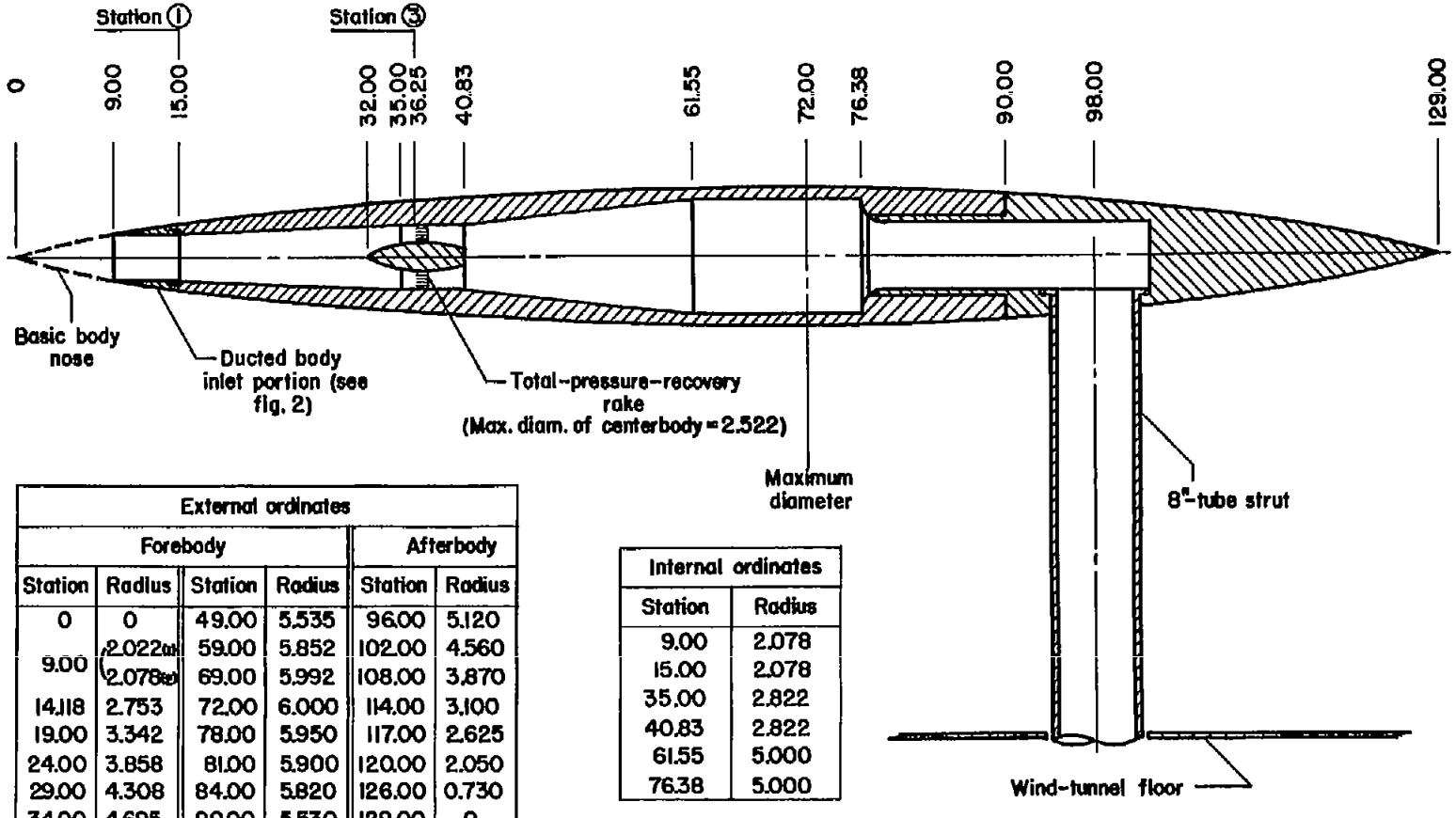

External ordinates					
Forebody				Afterbody	
Station	Radius	Station	Radius	Station	Radius
0	0	49.00	5.535	96.00	5.120
9.00	2.022(a) 2.078(b)	59.00	5.852	102.00	4.560
		69.00	5.992	108.00	3.870
14.118	2.753	72.00	6.000	114.00	3.100
19.00	3.342	78.00	5.950	117.00	2.625
24.00	3.858	81.00	5.900	120.00	2.050
29.00	4.308	84.00	5.820	126.00	0.730
34.00	4.695	90.00	5.530	129.00	0
39.00	5.028				

(a) Basic body
(b) Ducted body

Internal ordinates	
Station	Radius
9.00	2.078
15.00	2.078
35.00	2.822
40.83	2.822
61.55	5.000
76.38	5.000

Figure 1.- Model details. (All dimensions in inches.)

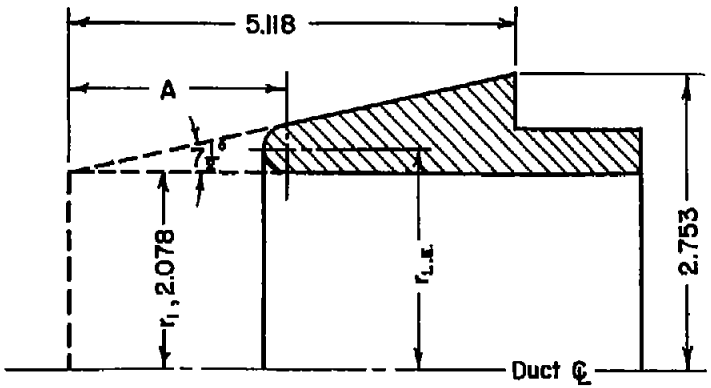

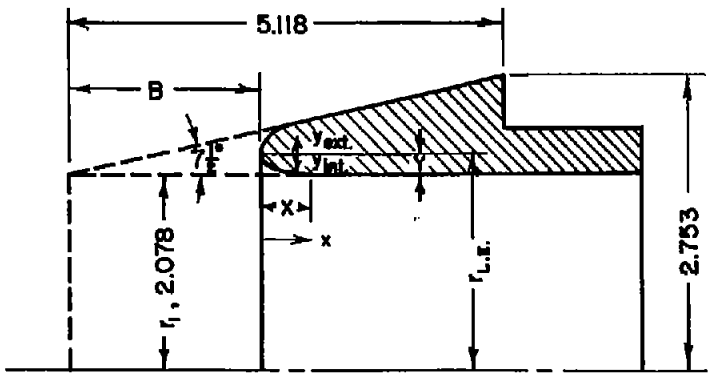

Circular lip dimensions				
Lip designation	Lip radius	A	$r_{L.E.}$	Contraction ratio $r^2_{L.E.}/r_i^2$
0	0	0	2.078	1.000
16R	0.16	2.44	2.238	1.158
33R	0.32	4.88	2.398	1.330

All dimensions in inches.

Elliptical lip dimensions (Y/X = 0.2777)					
Lip designation	Y	X	B	$r_{L.E.}$	Contraction ratio $r^2_{L.E.}/r_i^2$
8E	0.080	0.288	1.130	2.158	1.078
18E	0.176	0.632	2.500	2.254	1.177

Lip coordinates					
x/X	y/Y		x/X	y/Y	
	Internal	External		Internal	External
0	0	0	0.333	0.747	0.911
0.007	0.120	0.133	.445	.834	1.031
.019	.194	.227	.556	.894	1.128
.037	.267	.314	.704	.954	
.046	.300	.352	.741	.962	
.111	.460	.534	.852	.988	
.185	.580	.695	1.000	1.000	
.259	.675	.809			

Figure 2.- Inlet details.

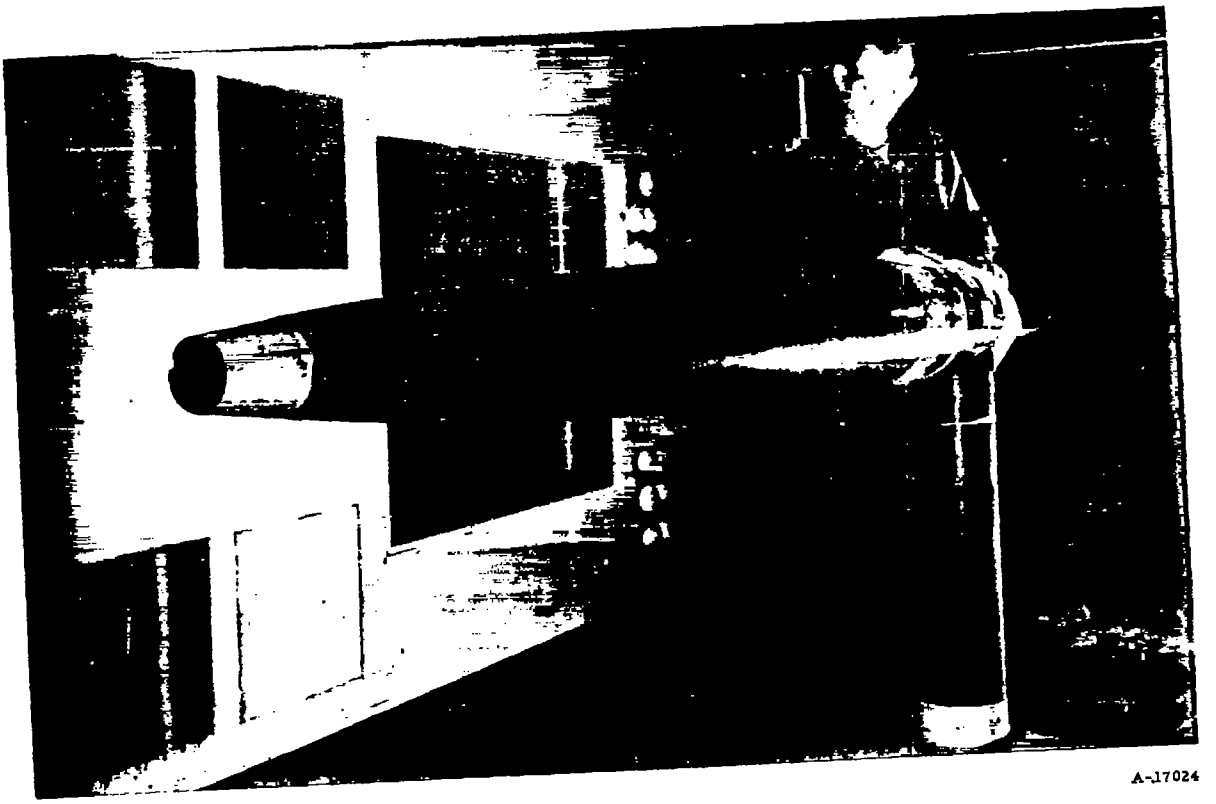

Figure 3.- Photograph of the model installed in the Ames 7- by 10-foot wind tunnel.

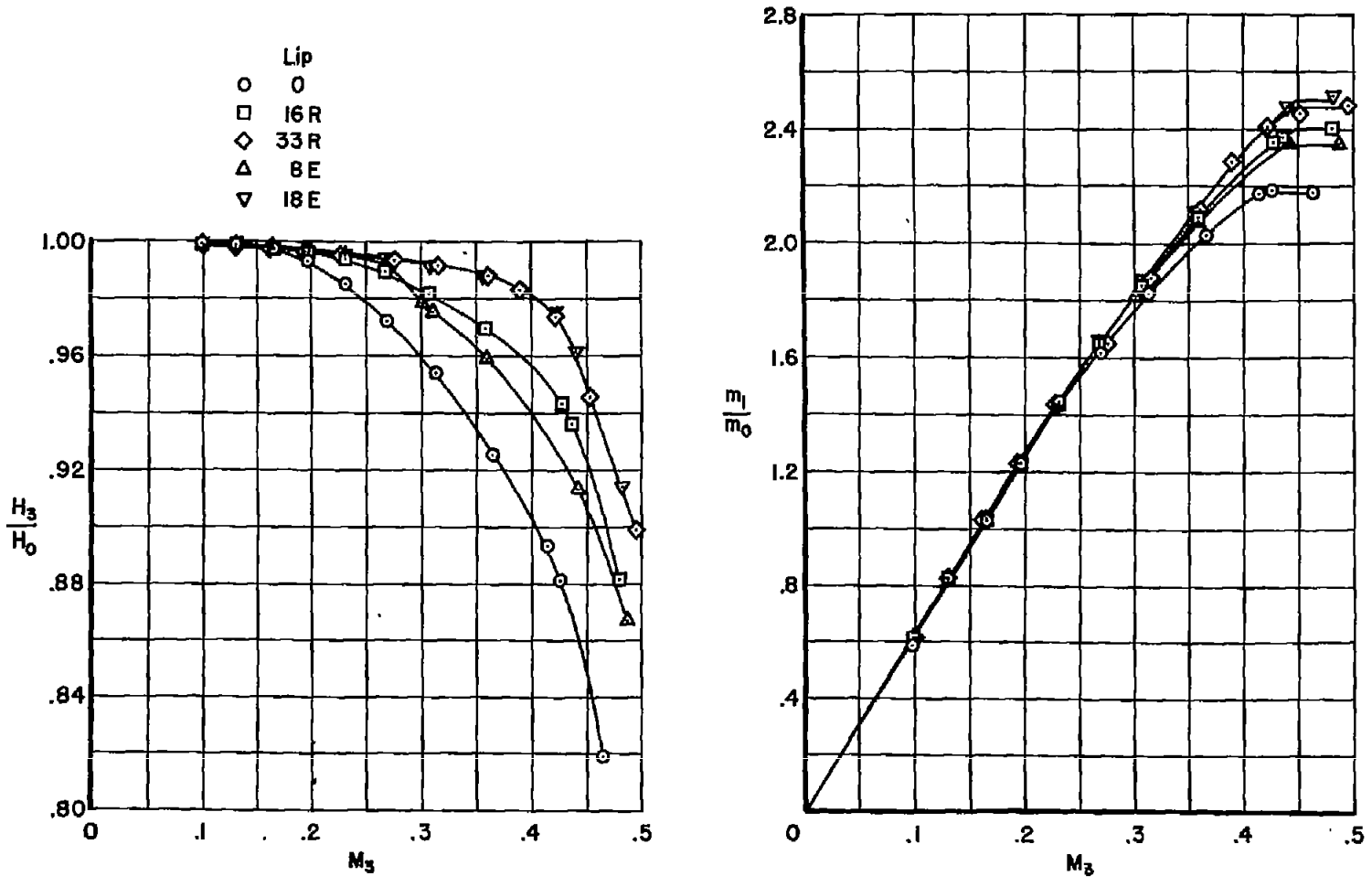

(a) $\alpha = 0^{\circ}$

Figure 4.- The variations of total-pressure ratio and mass-flow ratio with compressor-entrance Mach number for each of the lips and each angle of attack.

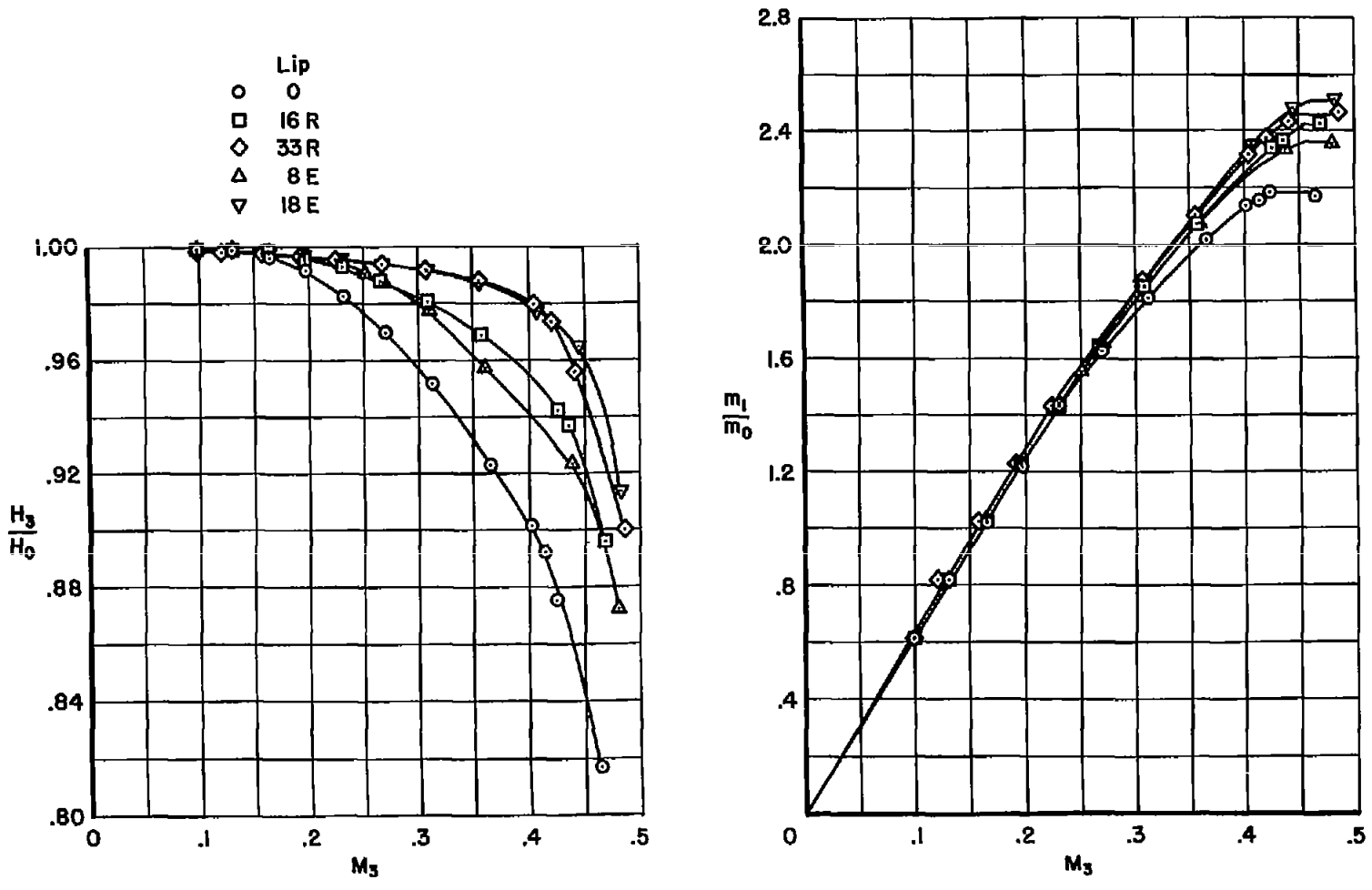

(b) $\alpha = 5^\circ$

Figure 4.- Continued.

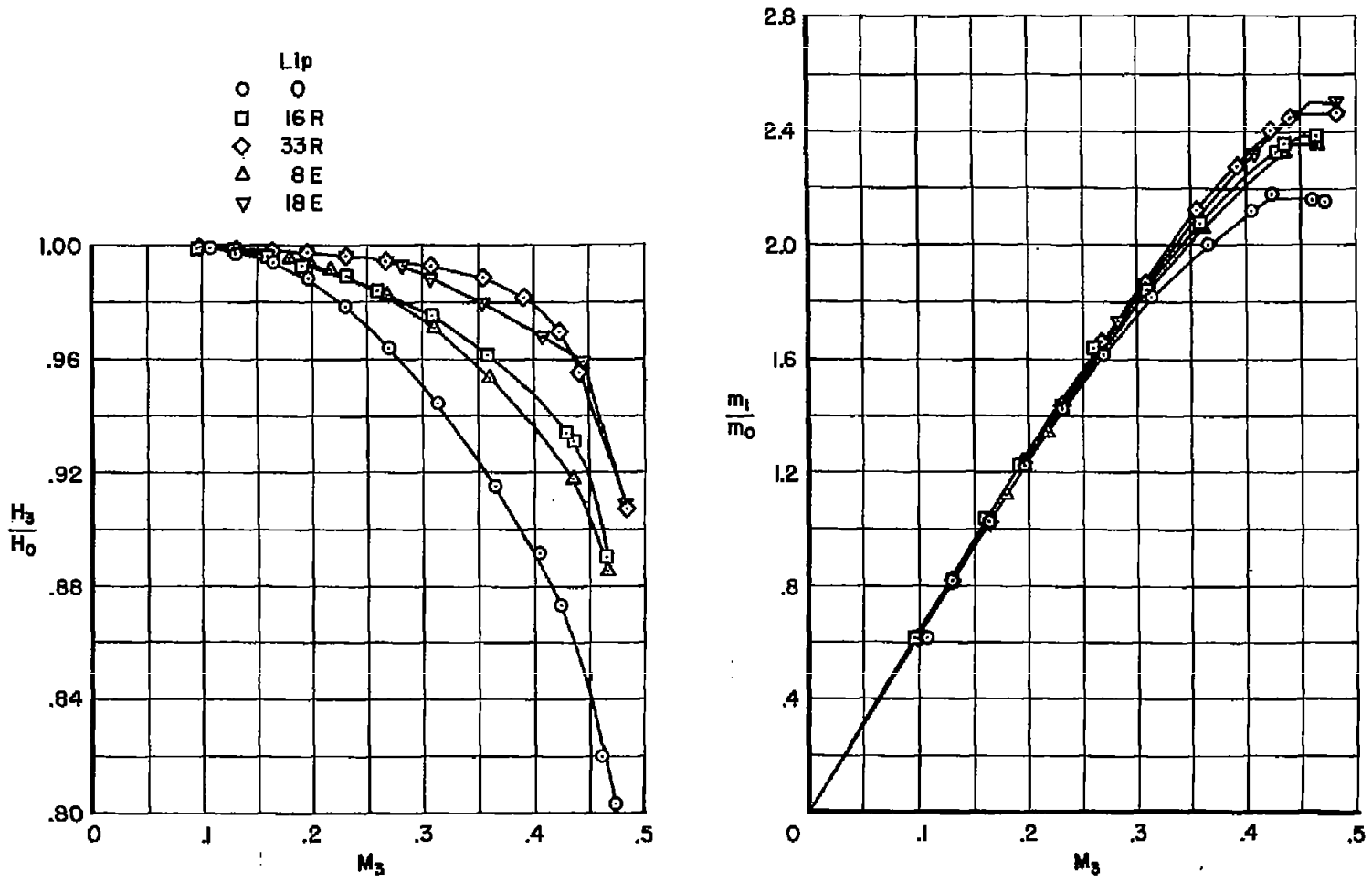

(c) $\alpha = 10^{\circ}$

Figure 4.- Continued.

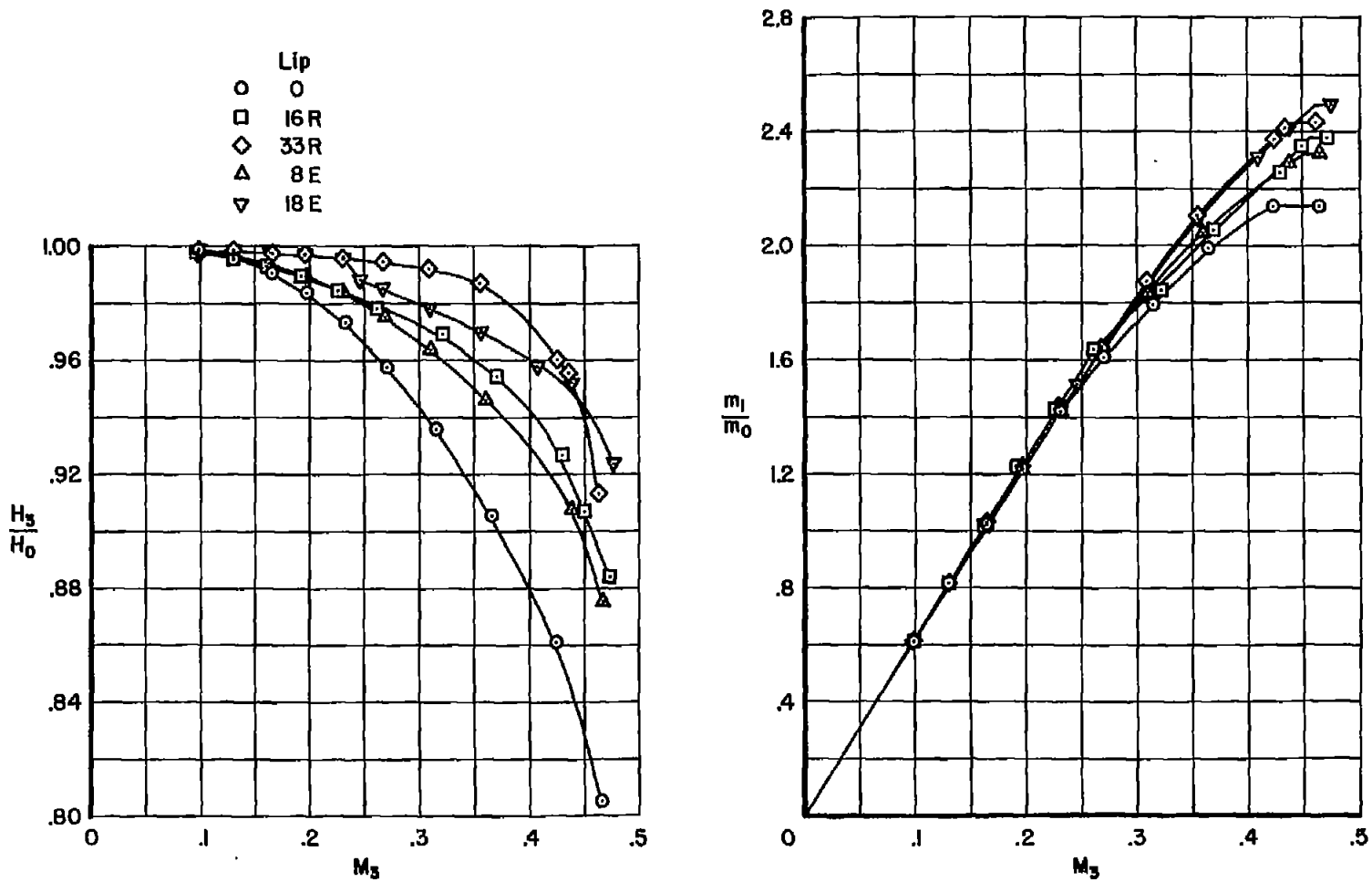

(d) $\alpha = 15^\circ$

Figure 4.- Continued.

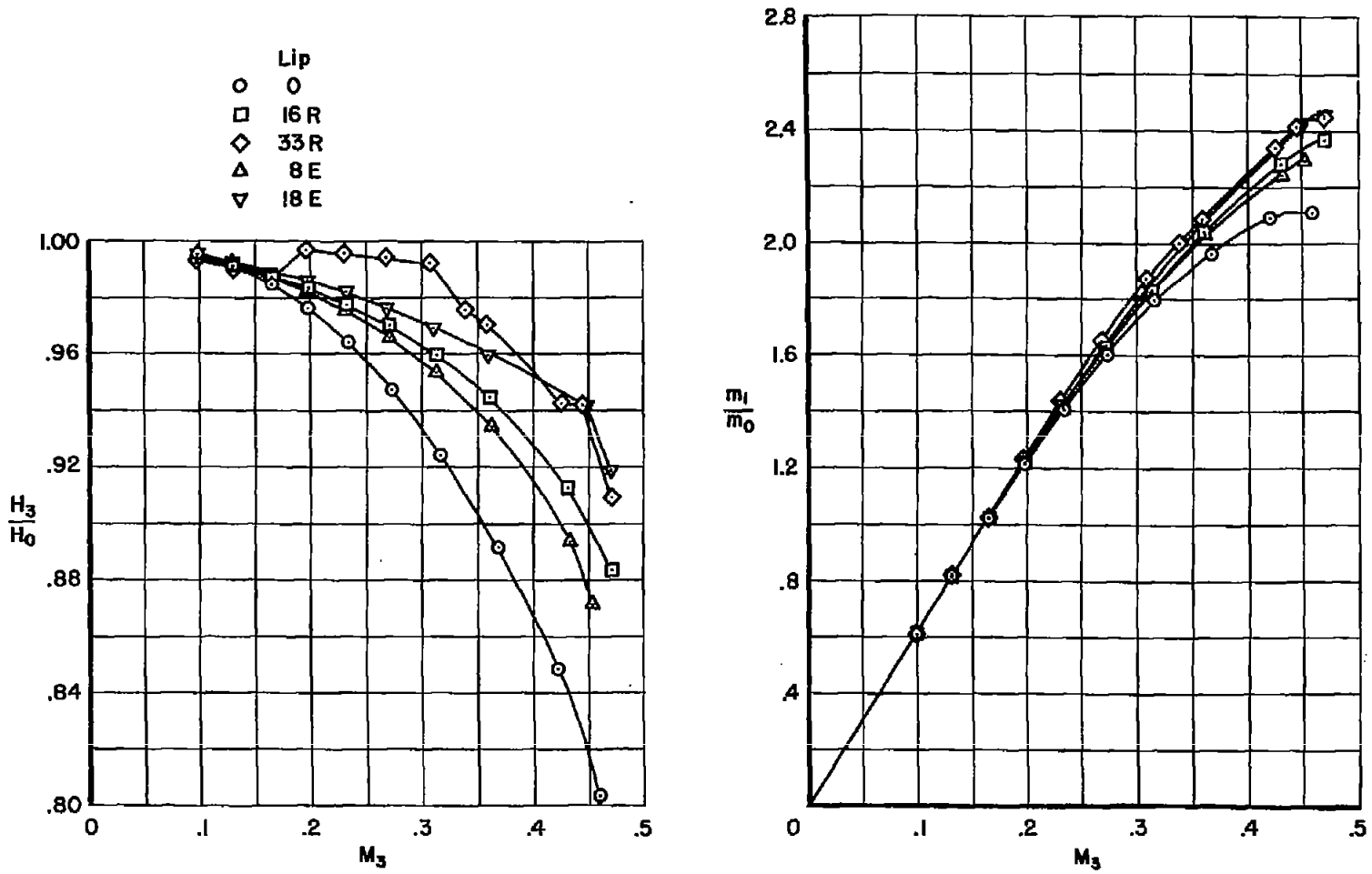

(e) $\alpha = 20^\circ$

Figure 4.- Continued.

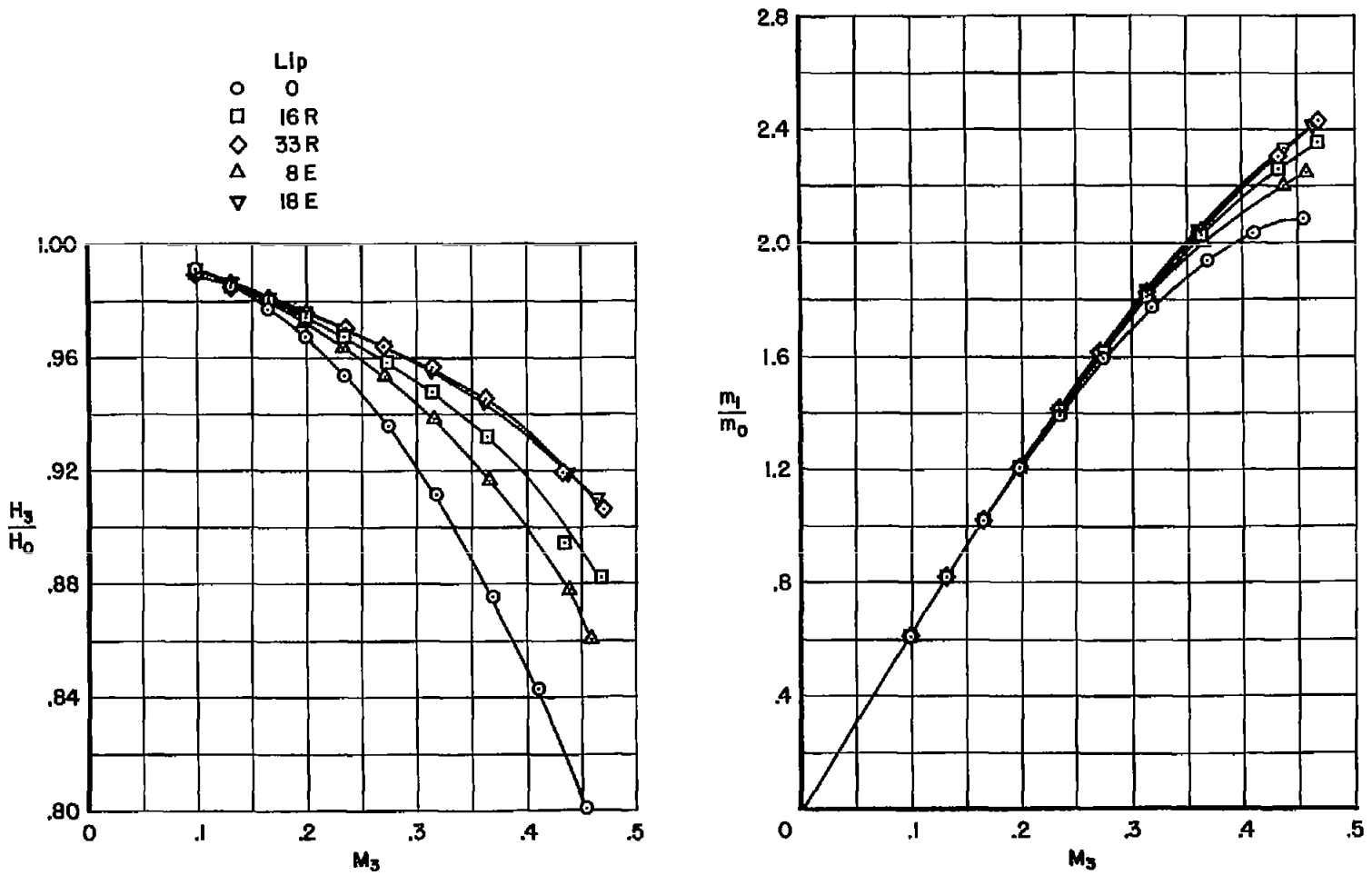

(f) $\alpha = 25^\circ$

Figure 4.- Concluded.

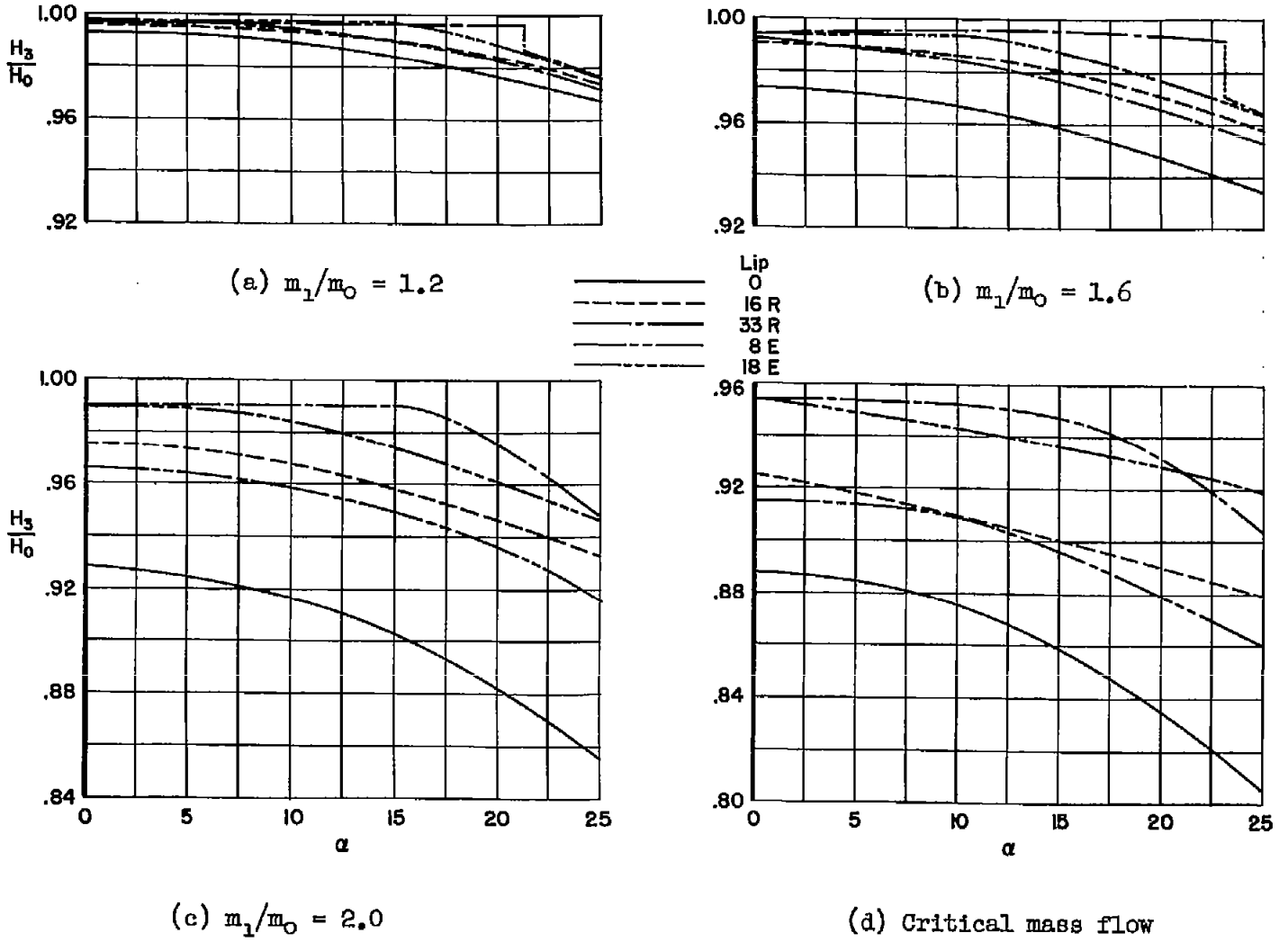

Figure 5.- The variation of total-pressure ratio with angle of attack for each of the lips for several mass-flow ratios.

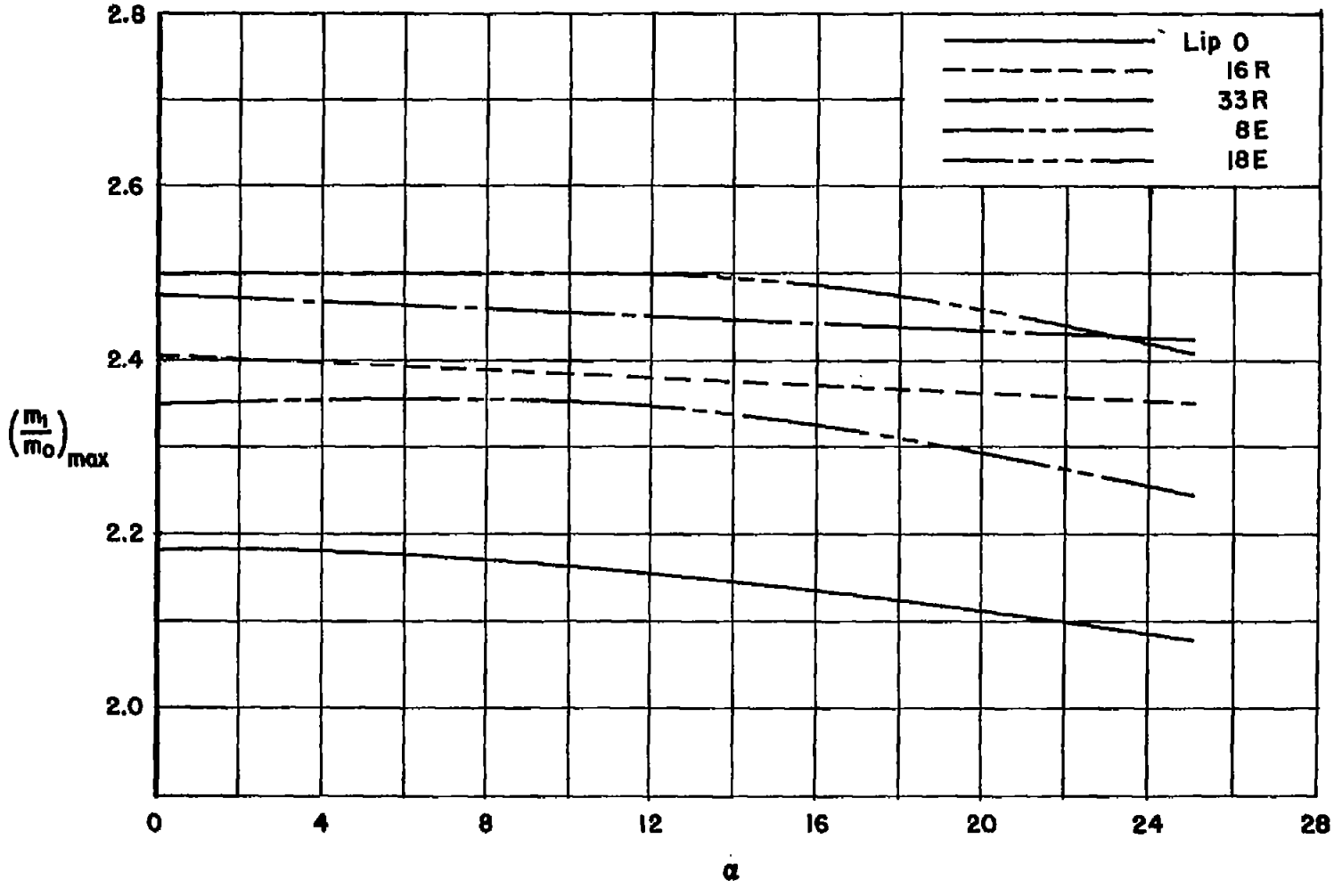

Figure 6. The variation of maximum mass-flow ratio with angle of attack for each of the lips.

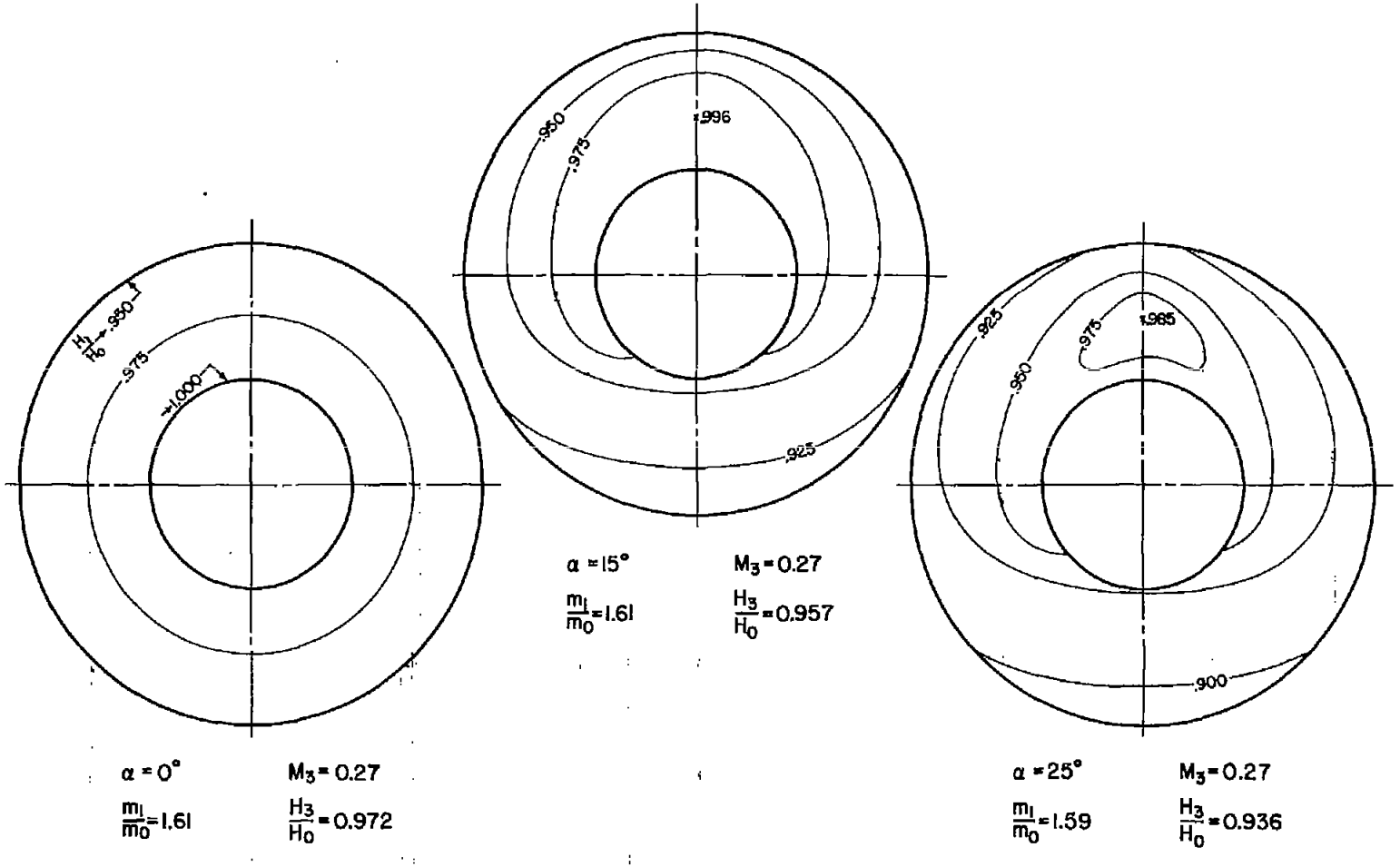

(a) Lip 0

Figure 7.- Typical contours of total-pressure ratio at the simulated engine-compressor entrance for each of the lips for $m_1/m_0 \approx 1.6$; contour interval = 0.025. (The top of the figures corresponds with the leeward side of the model.)

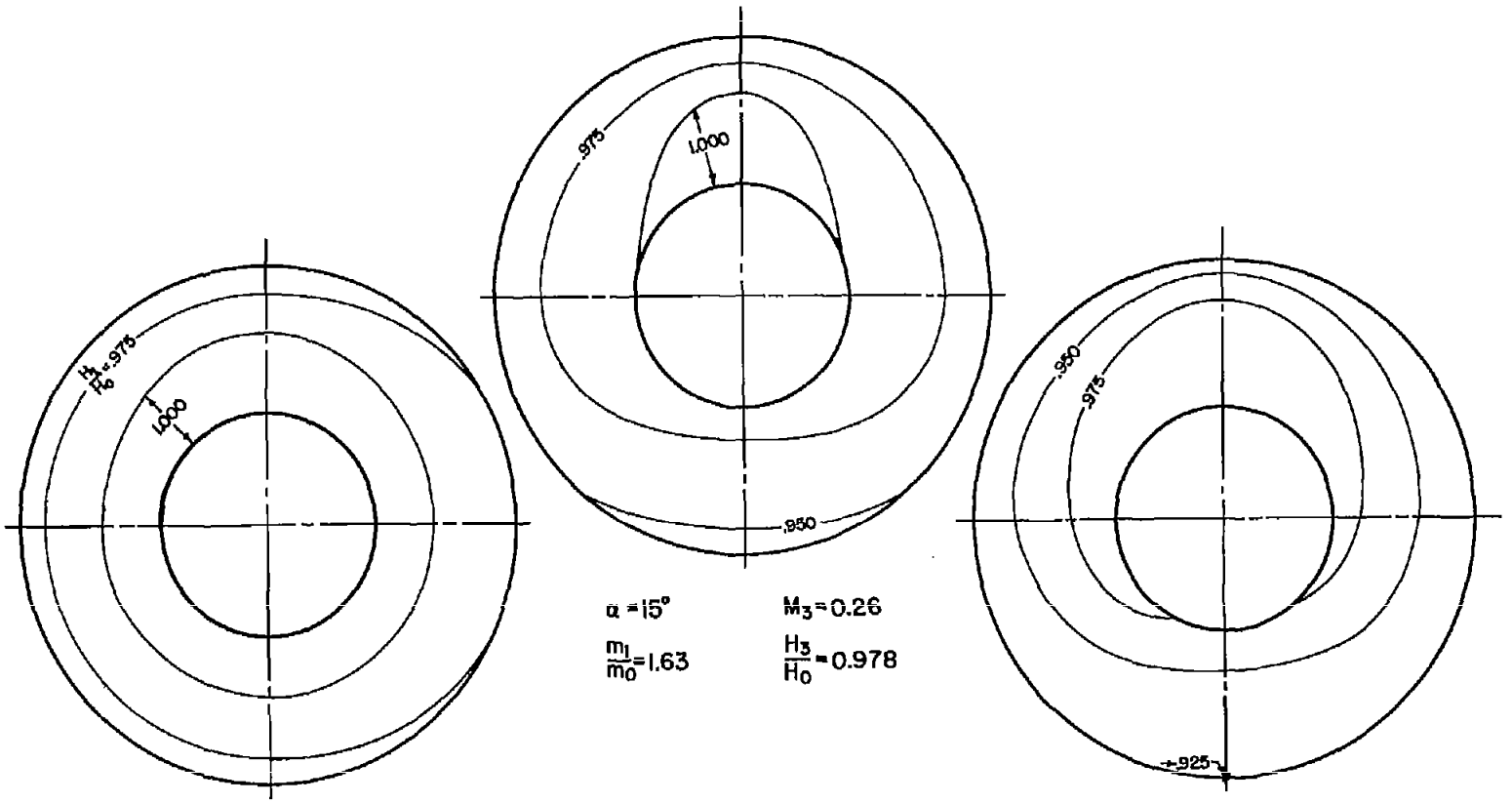

(b) Lip 16R

Figure 7.- Continued.

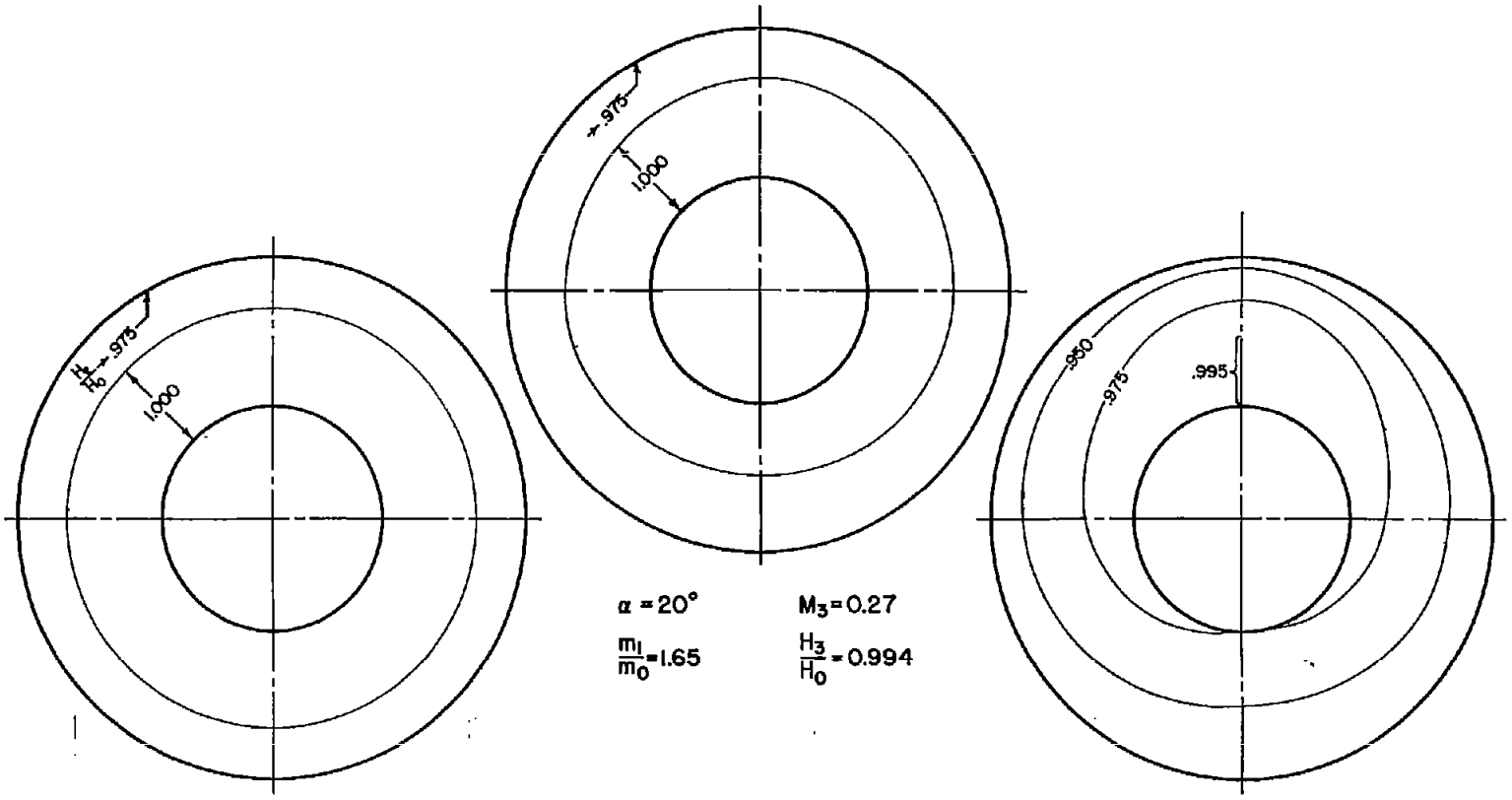

(c) Lip 33R

Figure 7.- Continued.

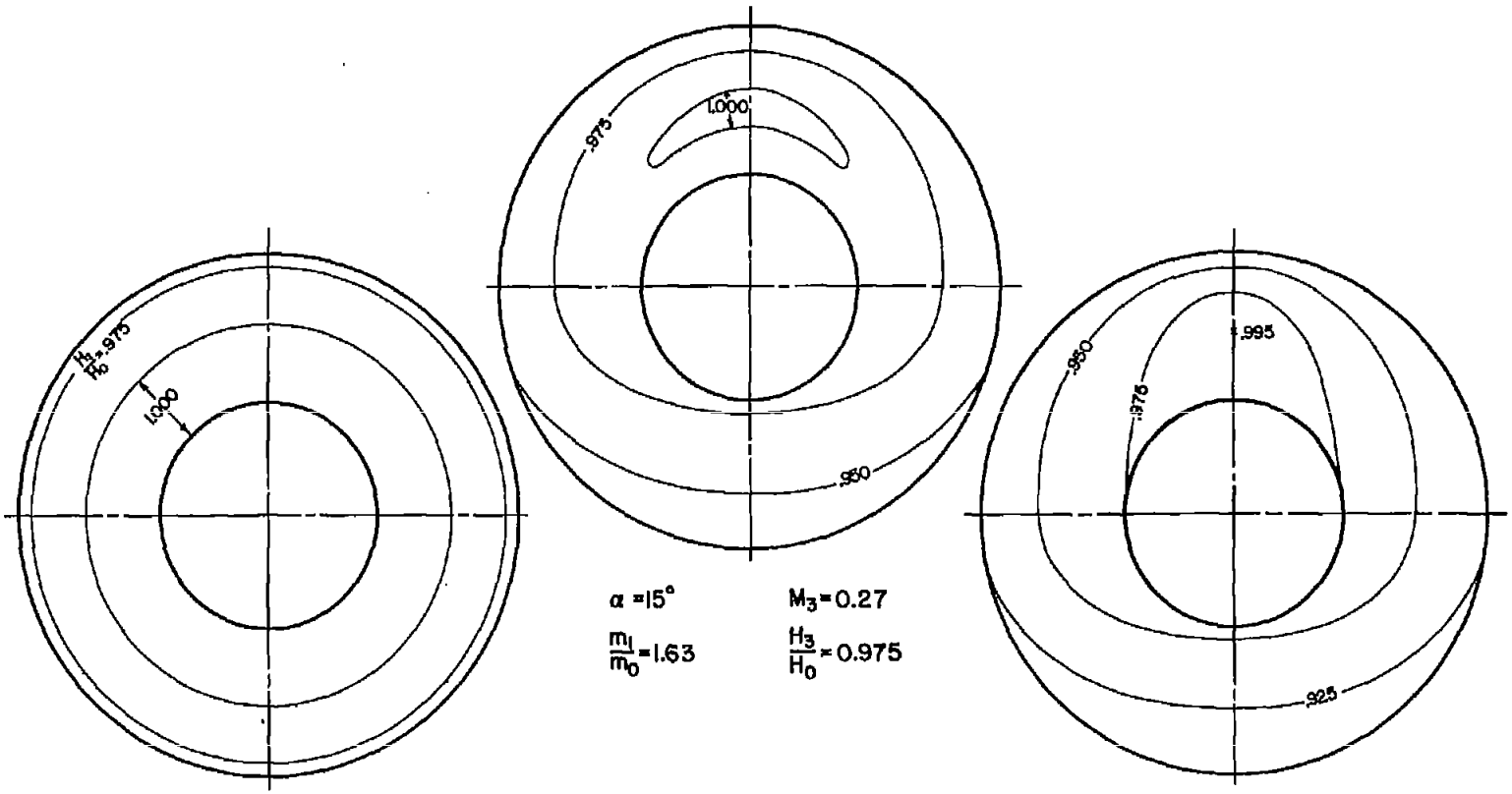

$\alpha = 0°$ $M_3 = 0.27$ $\frac{m_1}{m_0} = 1.64$ $\frac{H_3}{H_0} = 0.993$

$\alpha = 15°$ $M_3 = 0.27$ $\frac{m_1}{m_0} = 1.63$ $\frac{H_3}{H_0} = 0.975$

$\alpha = 25°$ $M_3 = 0.27$ $\frac{m_1}{m_0} = 1.60$ $\frac{H_3}{H_0} = 0.953$

(d) Lip 8E

Figure 7.- Continued.

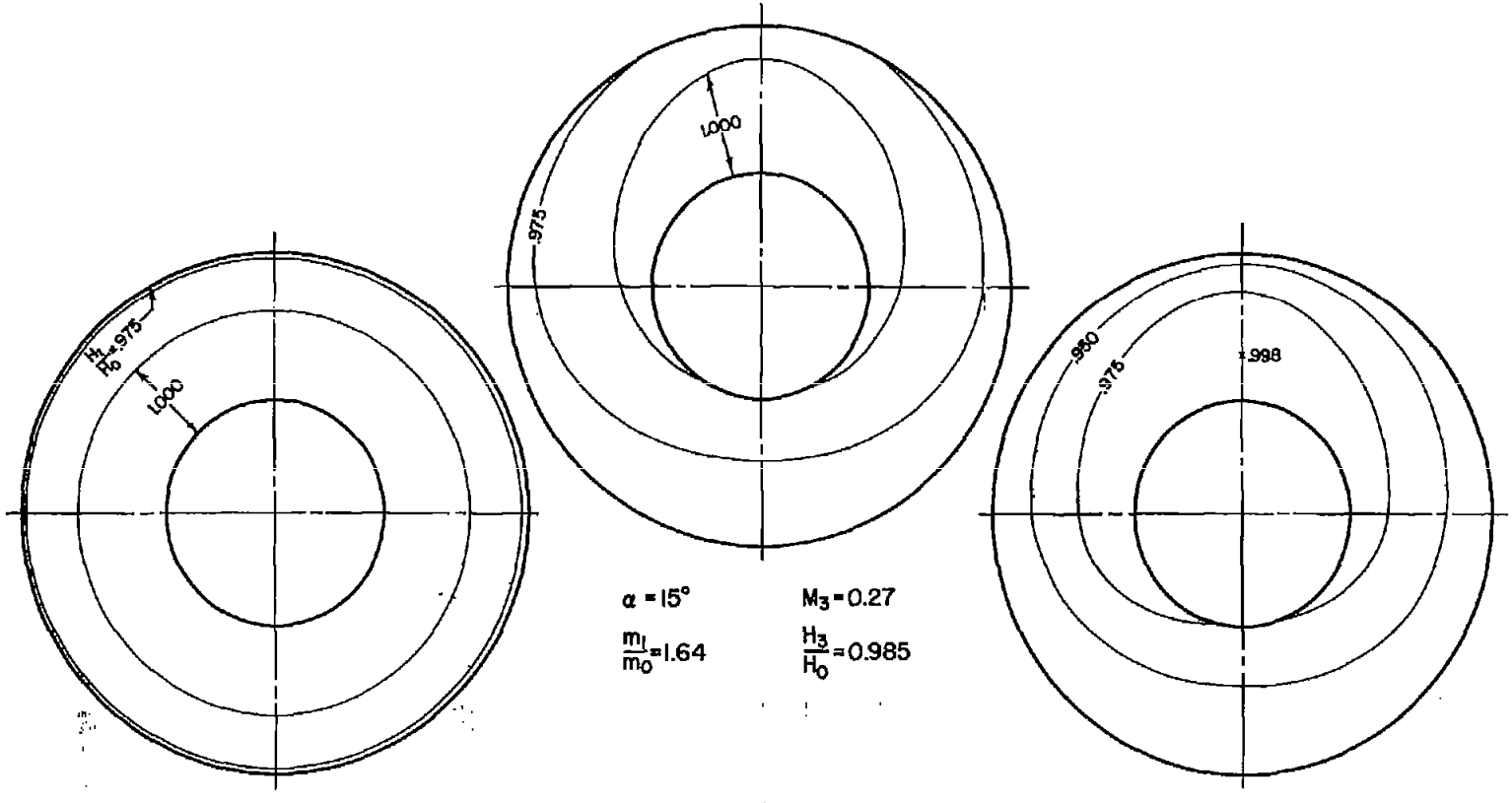

(e) Lip 18E

Figure 7.- Concluded.

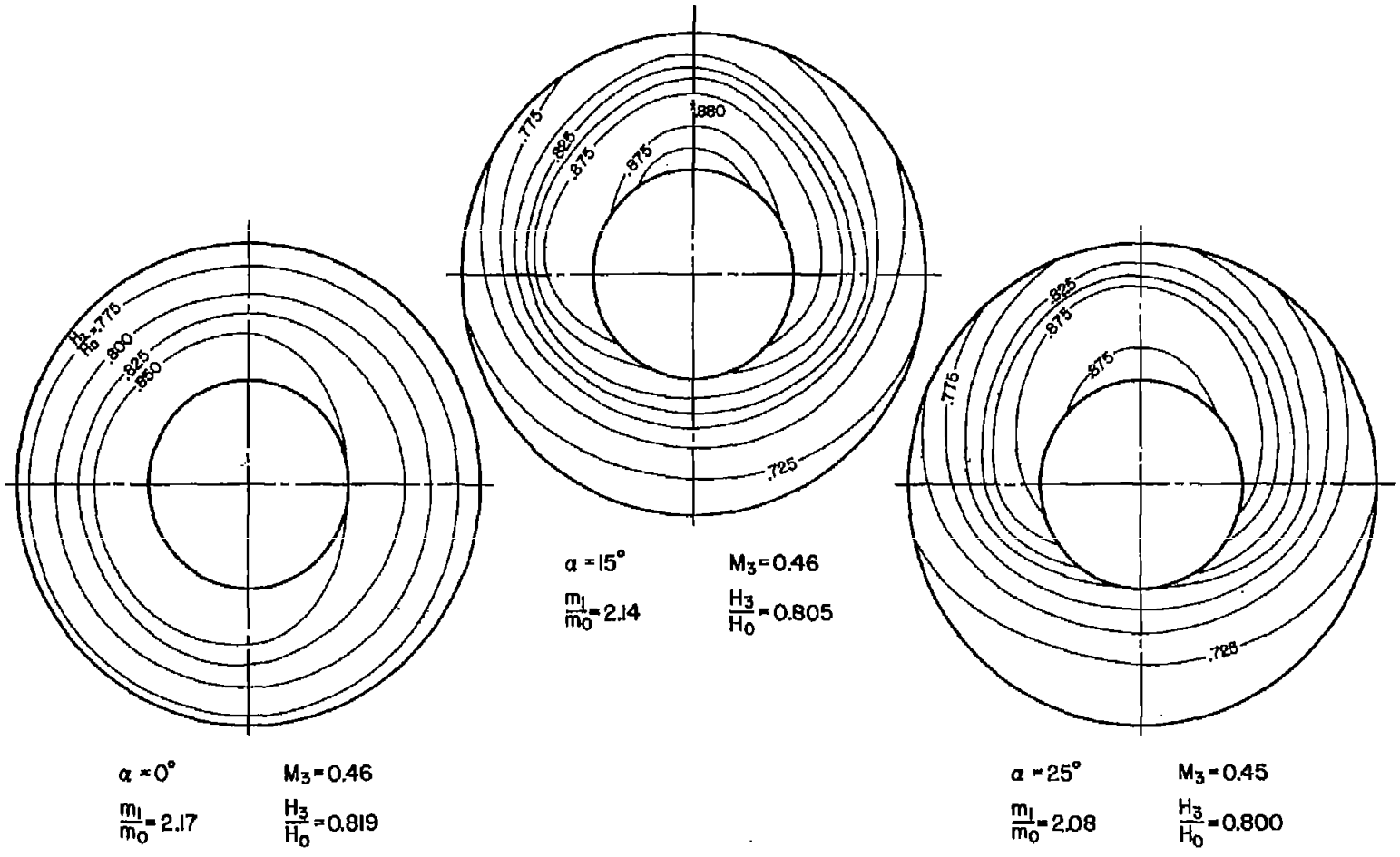

(a) Lip 0

Figure 8.- Typical contours of total-pressure ratio at the simulated engine-compressor entrance for each of the lips for critical mass-flow conditions; contour interval = 0.025. (The top of the figures corresponds with the leeward side of the model.)

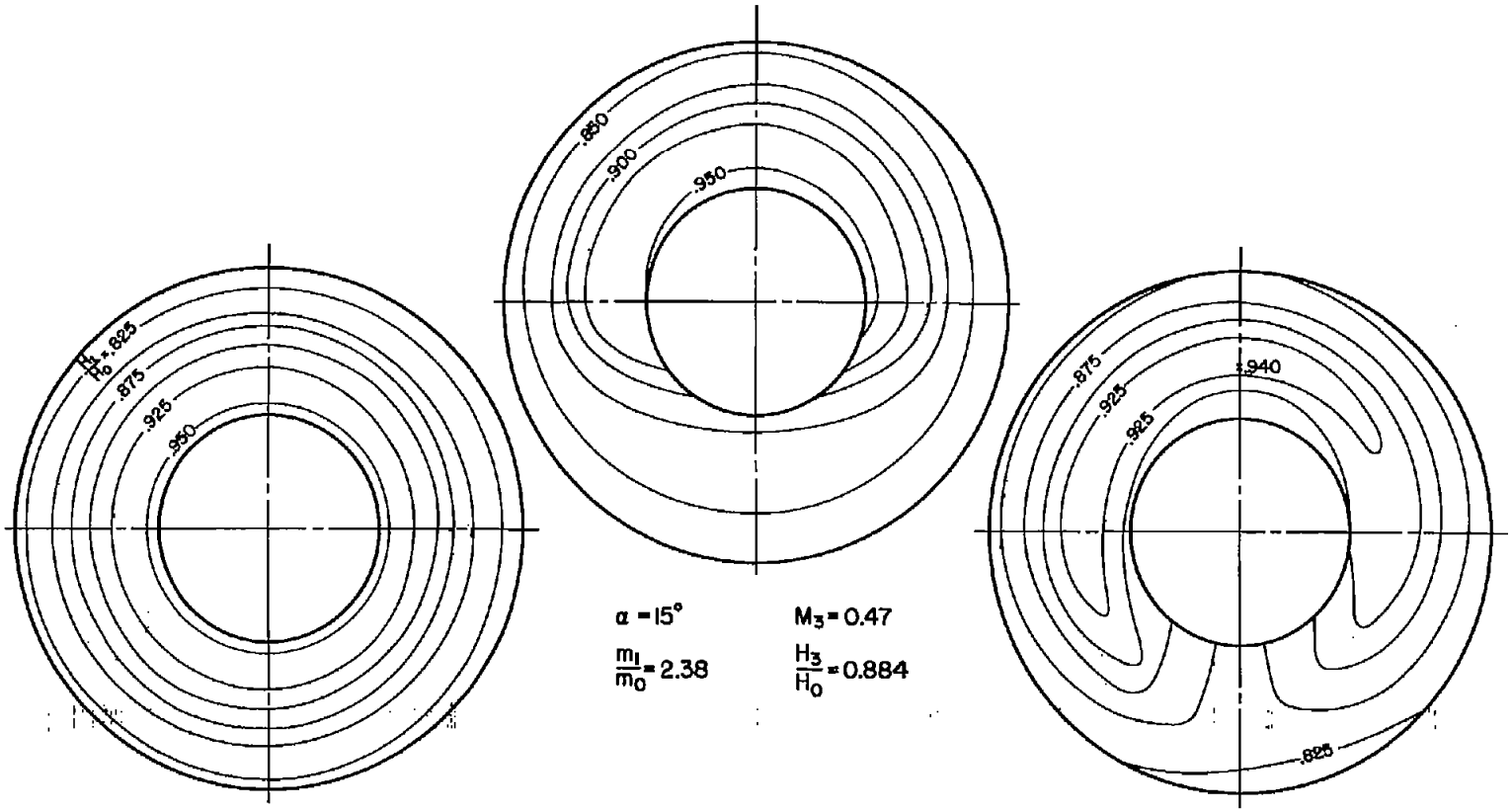

(b) Lip 16R

Figure 8.- Continued.

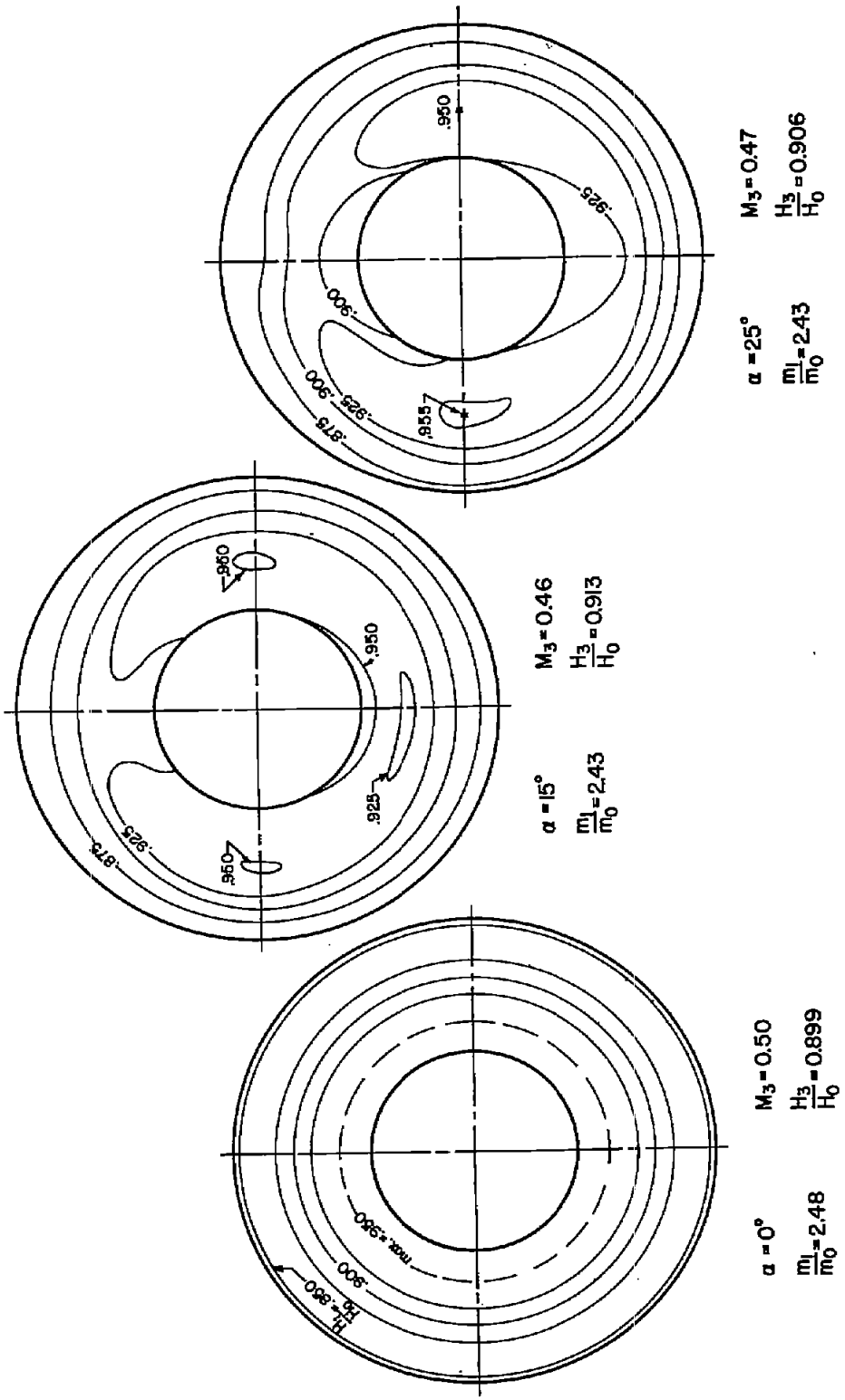

(c) Lip 33R

Figure 8.- Continued.

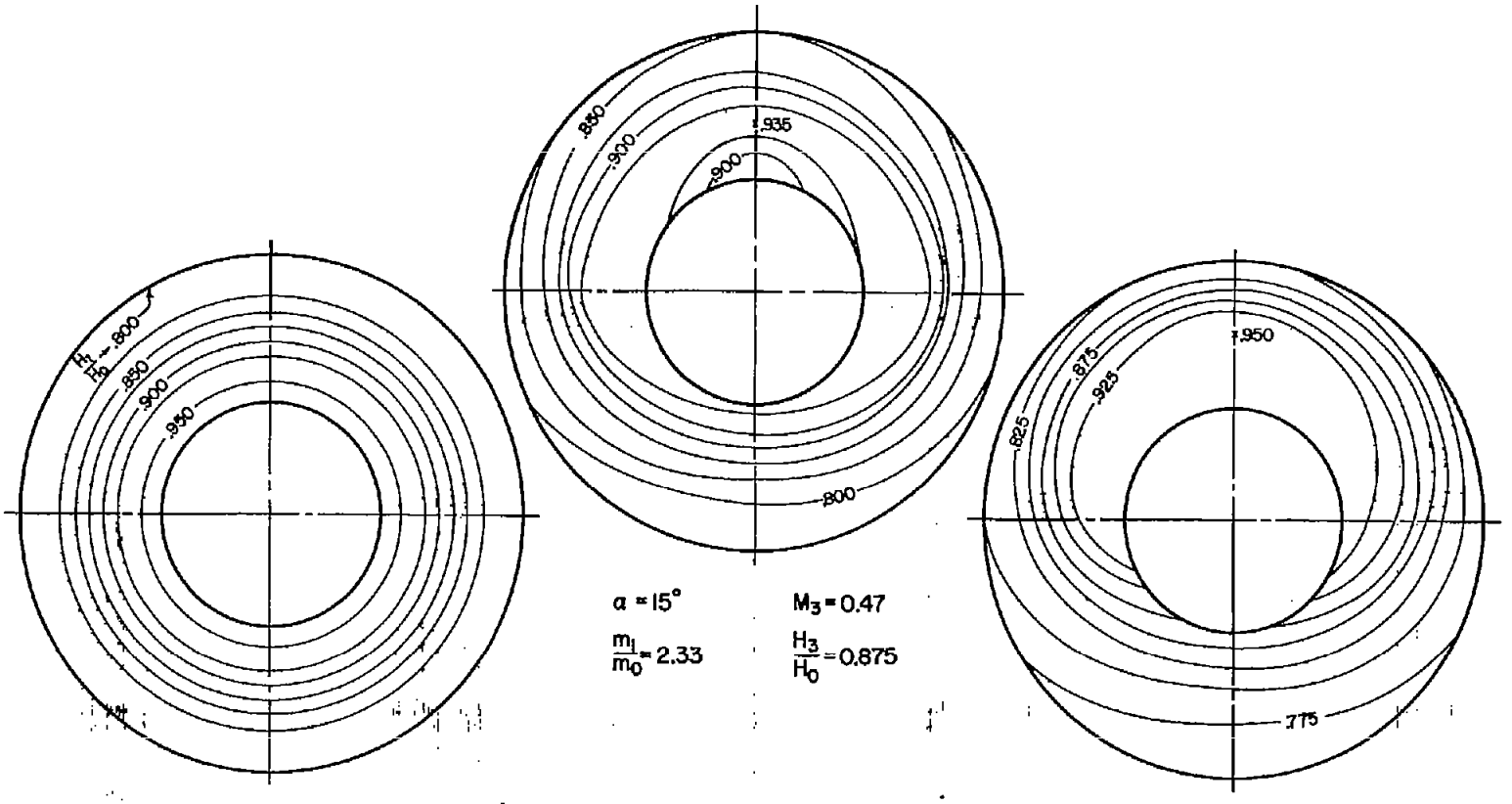

(d) Lip 8E

Figure 8.- Continued.

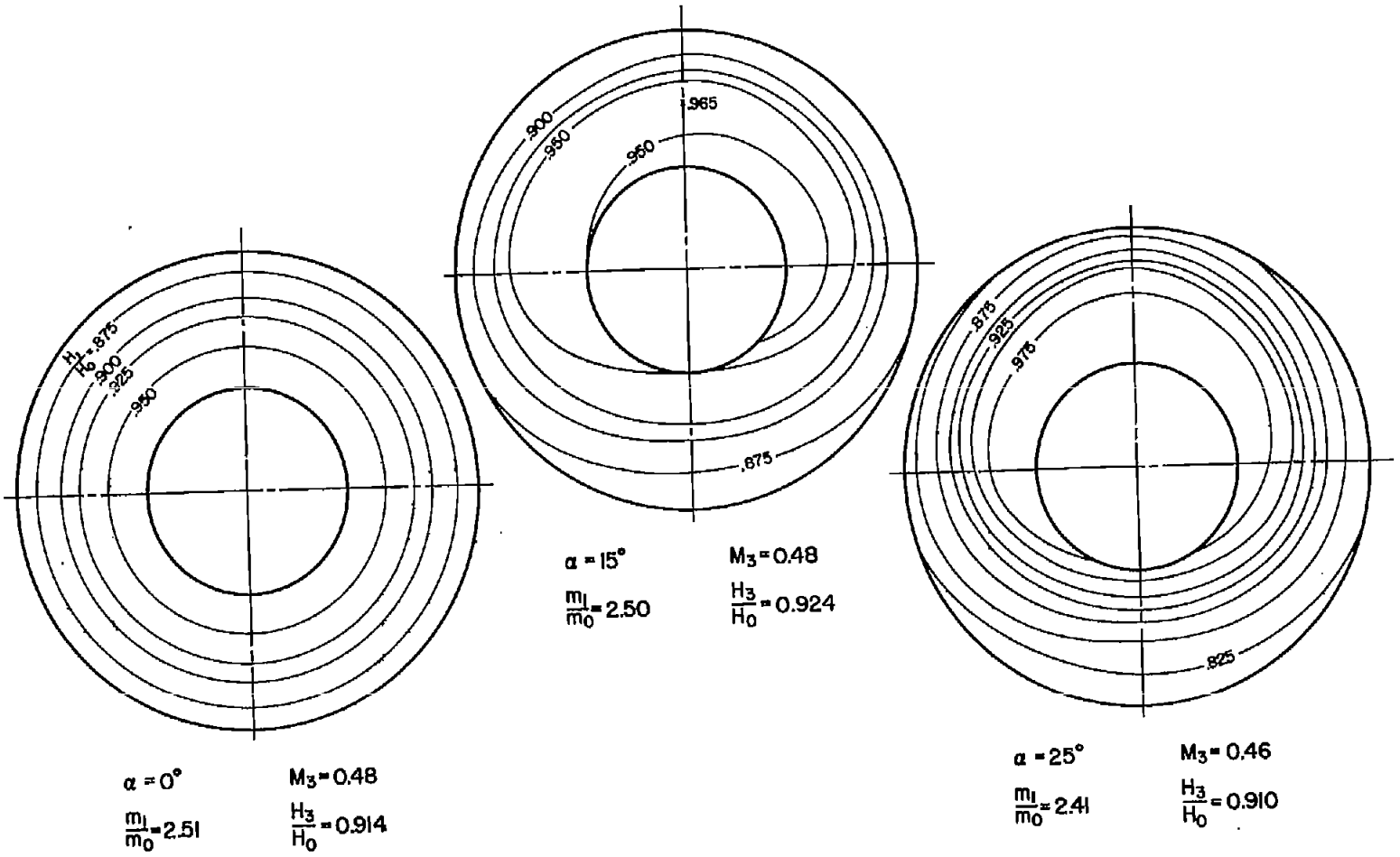

(e) Lip 18E

Figure 8.- Concluded.

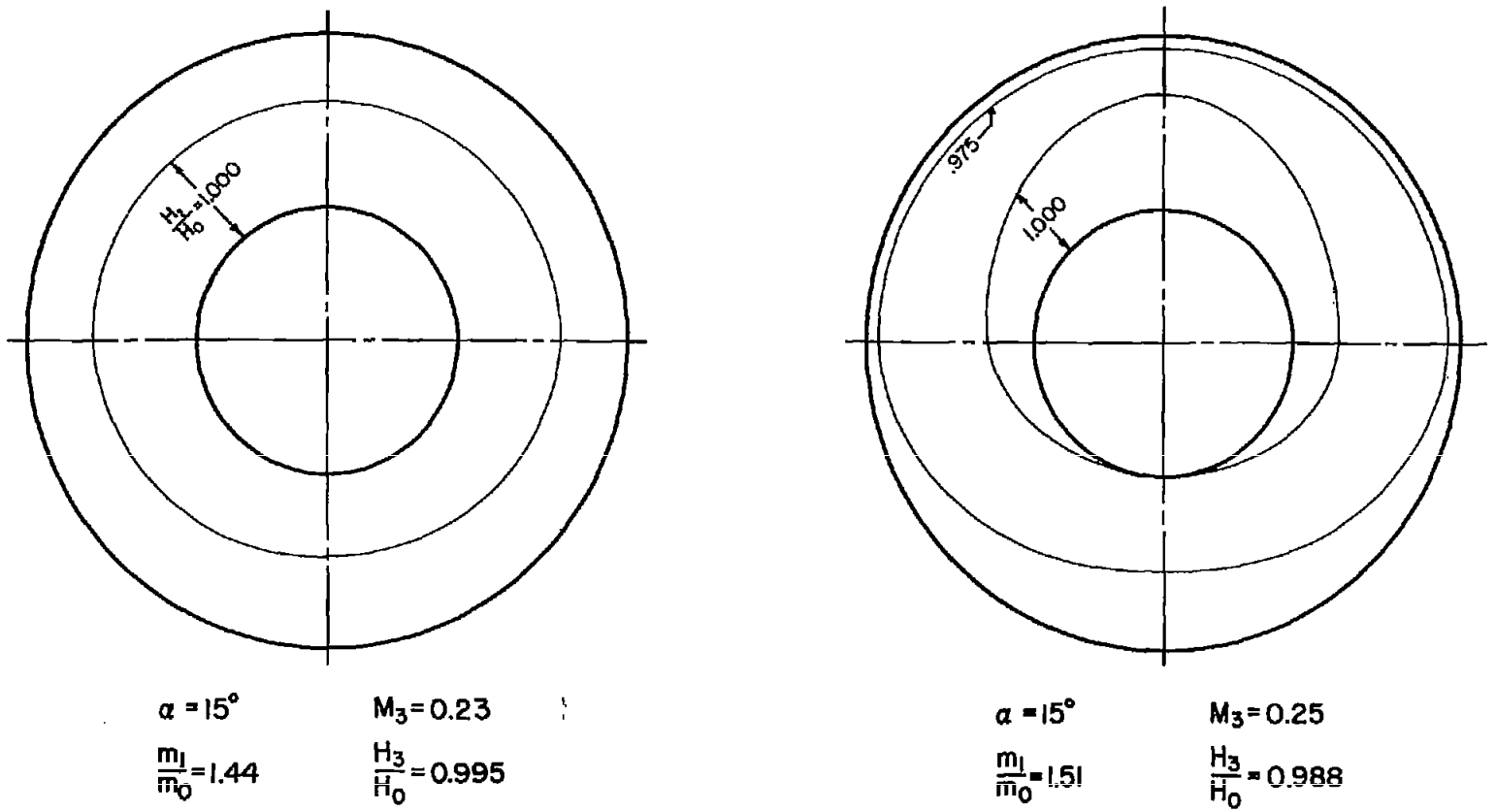

Figure 9.- Contours of total-pressure ratio at the simulated engine-compressor entrance for the model with lip 18E illustrating change of distribution accompanying separation from the lower lip at an angle of attack of 15°; contour interval = 0.025. (The top of the figures corresponds with the leeward side of the model.)

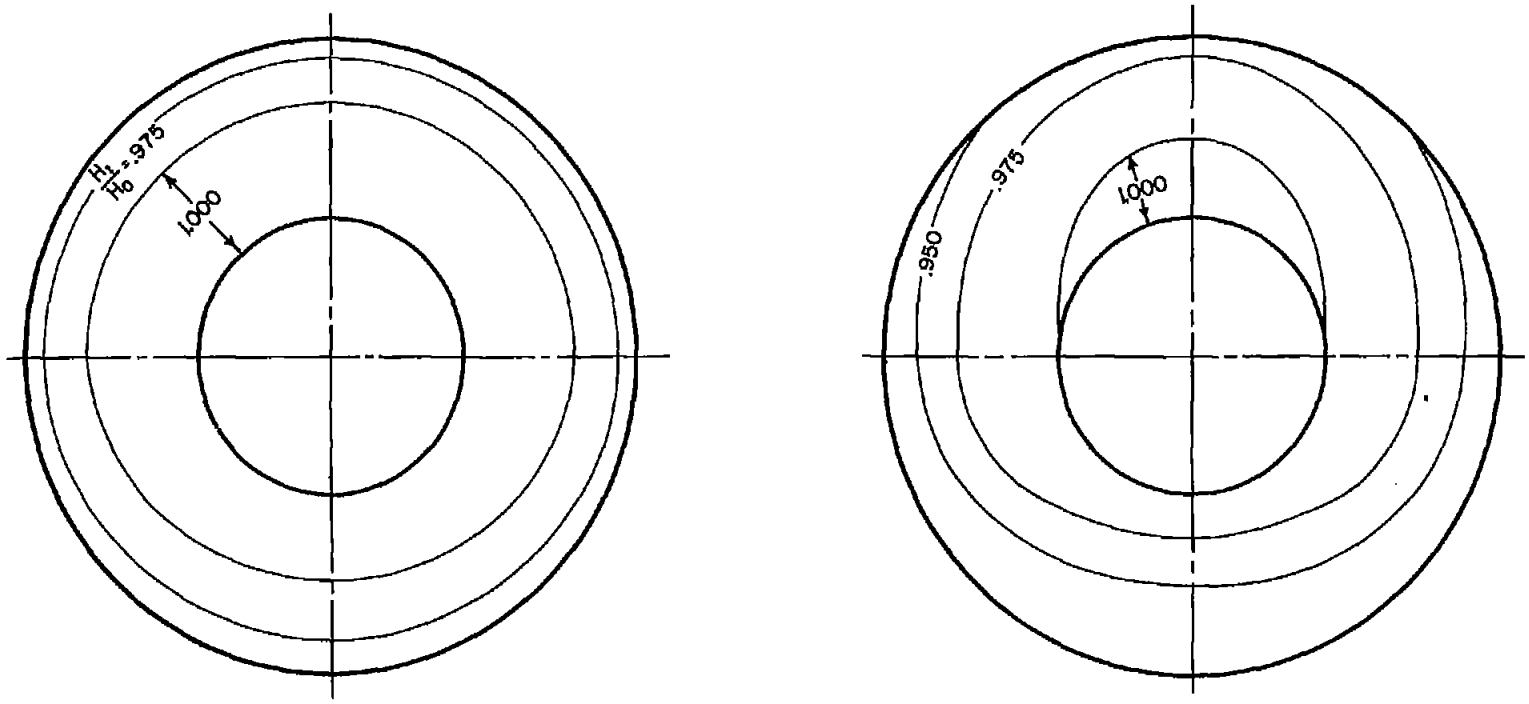

$\alpha = 20°$ $M_3 = 0.31$

$\frac{m_1}{m_0} = 1.87$ $\frac{H_3}{H_0} = 0.992$

$\alpha = 20°$ $M_3 = 0.36$

$\frac{m_1}{m_0} = 2.08$ $\frac{H_3}{H_0} = 0.970$

Figure 10.- Contours of total-pressure ratio at the simulated engine-compressor entrance for the model with lip 33R illustrating the change of distribution accompanying separation from the lower lip at an angle of attack of 20°; contour interval = 0.025. (The top of the figures corresponds with the leeward side of the model.)

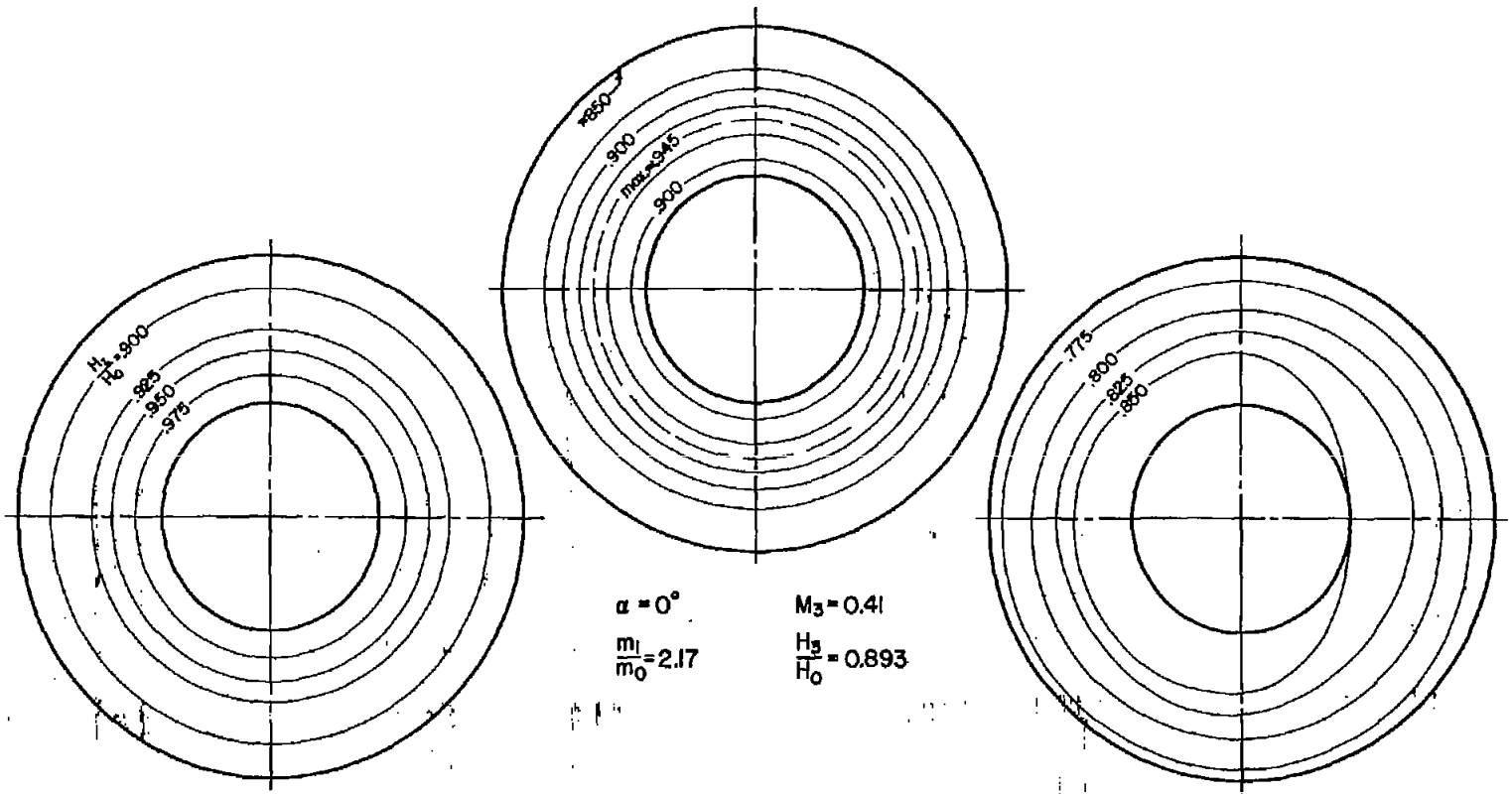

Figure 11.- Contours of total-pressure ratio at the simulated engine-compressor entrance for the model with lip 0 illustrating the change of distribution during choked operation at an angle of 0°; contour interval = 0.025.

NACA-Langley - 5-17-55 - 1000